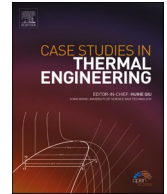




Contents lists available at ScienceDirect

Case Studies in Thermal Engineering

journal homepage: www.elsevier.com/locate/csite

Thermodynamic and economic analysis of ocean thermal energy conversion system using zeotropic mixtures

Yanmei Zhang^a, Jiawei Deng^b, Zilong Deng^{b,*}

^a Shanghai Electric Group Co., Ltd., Shanghai, 200070, PR China

^b School of Energy and Environment, Southeast University, Nanjing, 210096, PR China

ARTICLE INFO

Keywords:

Ocean thermal energy conversion
Zeotropic mixtures
Thermodynamic
Economic
Levelized cost of electricity

ABSTRACT

Zeotropic mixtures offer a promising strategy for enhancing the thermodynamic efficiency and economic feasibility of ocean thermal energy conversion (OTEC) systems. This study investigates two binary mixtures containing R32: R32/R125 and R32/R134a. Through the development of comprehensive thermodynamic and economic models, the research examines the impact of mass fraction and evaporation temperature on the efficiency and cost-effectiveness of the OTEC system. The results indicate that, especially at high evaporation temperatures, the R32/R134a mixture—characterized by significant temperature glide—substantially increases the total energy production capacity of the OTEC system. Compared to pure R32, the OTEC with R32/R134a (mass fraction of R32 is 0.55) has a net output power increase of 9.87 kW and a reduction in LCOE of about 61.4%. In addition, the advantages of R32/R125 mixtures over pure working fluids are not significant due to the small glide temperature. Ultimately, this investigation enhances the overall performance of OTEC systems, thereby supporting sustainable energy solutions for island communities.

Nomenclature

Abbreviations

GWP	Global warming potential
ODP	Ozone depletion potential
ORC	Organic Rankine cycle
OTEC	Ocean thermal energy conversion
Symbols	
A	Area, m ²
$B_1, B_2, C_1, C_2, C_3, K_1, K_2, K_3$	Costing-related constants, -
c	Specific heat, kJ/(kg·K)
C	Cost, \$
CEPCI	Chemical Engineering Plant Cost Index, -
COM	Operational and maintenance costs, \$
D	Diameter, m
f	Fanning friction factor, -
f_B	Total loss coefficient, -
F_M	Material factor, -

t_{op}	Time of operation, h
T	Temperature, °C
v	Velocity, m/s
W	Power, kW

Greek letters

η	Efficiency, %
Δ	Difference, -
ρ	Density, kg/m ³

Subscripts

0,1,2 ...	Nodes in system
B	Bend pipe
C	Condenser
cs	Cold seawater
d	Density
E	Evaporator
HX	Heat Exchanger
in	Inlet

(continued on next page)

* Corresponding author.

E-mail address: zldeng@seu.edu.cn (Z. Deng).

<https://doi.org/10.1016/j.csite.2024.105408>

Received 22 July 2024; Received in revised form 5 October 2024; Accepted 2 November 2024

Available online 12 November 2024

2214-157X/© 2024 The Authors. Published by Elsevier Ltd. This is an open access article under the CC BY-NC license (<http://creativecommons.org/licenses/by-nc/4.0/>).

(continued)

F_p	Pressure factor, -	net	Net
F_s	Ancillary cost factor, -	out	Outlet
g	Gravitational acceleration, m/s^2	p	Pump
h	Specific enthalpy, kJ/kg	P	Pipeline
ir	Annual interest rate, -	ref	Reference
K	Absolute roughness, m	s	Isentropic
L	Length, m	SP	Straight pipe
$LCOE$	Levelized cost of electricity, $\$/kWh$	t	Turbine
L_t	Lifespan, year	tot	Total
m	Mass flow rate, kg/s	wf	Working fluid
p	Pressure, Pa	ws	Warm seawater
Q	Heat load, kW	WP	Seawater pipe
Re	Reynolds number, -		

1. Introduction

Ocean thermal energy conversion (OTEC) leverages the thermal variance between the ocean's warmer surface water and its colder deep-sea counterpart to produce electricity [1,2]. This approach is both sustainable and eco-friendly, offering a promising alternative for energy generation. It is widely regarded as a promising solution for providing a green, stable, and sustainable power supply to remote tropical islands [3–5]. However, due to the limitation of available temperature differences (generally lower than 25 °C), the efficiency of traditional OTEC system is relatively low [6,7]. Zeotropic mixtures, with their temperature glide characteristics, can significantly reduce irreversible losses, thereby enhancing the efficiency of OTEC systems [8,9]. Accordingly, studying zeotropic mixtures applied in the OTEC system is of great practical significance.

One of the major limiting factors for the application of OTEC is its low economic efficiency, primarily due to the low thermal efficiency caused by the small driving temperature difference [3]. Therefore, improving the thermal efficiency of OTEC systems is a key research direction, mainly focusing on optimizing cycle structures and working fluids [6]. OTEC was initially proposed as a Rankine cycle [10]. Later, the Kalina cycle [11], using ammonia water as the working fluid, and its modified form, the Uehara cycle [12], were introduced, significantly improving the thermal efficiency of OTEC. However, this improvement came at the cost of adding extra distillation and absorption units (due to incomplete evaporation of ammonia), increasing system investment and reducing reliability [13]. As a result, the simple and reliable Rankine cycle remains the preferred choice for OTEC engineering applications today. Another important approach to enhancing the thermal efficiency of OTEC systems is finding a suitable working fluid for the Rankine cycle. In most studies, R717 (ammonia) is considered the most suitable working fluid for Rankine cycle-based OTEC systems, primarily due to its higher latent heat and lower viscosity [14,15]. For example, Rosard [16] compared 11 working fluids for OTEC systems and found that R717 performed best in terms of turbine output. Sun et al.'s research [17] also identified R717 as the ideal working fluid for OTEC. Yoon et al. [18] screened various fluids, including dry, wet, and isentropic fluids, for subcritical OTEC systems and concluded that R717 had the best overall performance. However, they also noted that R717 poses issues due to its toxicity, flammability, and strong corrosiveness. Given these concerns, non-toxic, non-corrosive organic refrigerants may be the best alternative to R717. Some studies have demonstrated the thermodynamic advantages of organic refrigerants in OTEC systems [19]. For instance, Wu et al. [20] conducted extensive research comparing various organic refrigerants to R717, concluding that organic refrigerants outperformed R717 in terms of exergy efficiency. Gong et al. [21] evaluated the performance of six working fluids at different turbine inlet pressures, identifying R125, R143a, and R32 as suitable alternatives.

In Rankine cycles that employ pure substances as working fluids, the isothermal phase change characteristics of these fluids lead to temperature mismatches between the fluid in the evaporator and condenser, resulting in significant irreversible losses. This is one of the key reasons for the thermodynamic advantages of the Kalina and Uehara cycles, which use ammonia-water mixtures as working fluids [22]. By introducing zeotropic mixtures as the working fluids in a Rankine cycle, it is possible to enhance the system's thermodynamic performance while maintaining simplicity and reliability—on the condition that the zeotropic mixture is fully evaporated to avoid the need for additional equipment [23–25]. This principle has already been widely applied in the field of low-temperature waste heat recovery [26]. For instance, Liu et al. [27] proposed using an R600a/R601a mixture as the working fluid in a system designed for heat recovery from sources at 100–150 °C, achieving greater power output than using R600a alone. Similarly, Mosaffa et al. [28] evaluated organic working fluids for solar pond organic Rankine cycles, and found that a 0.6/0.4 mass ratio mixture of R245ca/R236ea delivered the best thermal performance. However, research on this approach in OTEC systems remains limited. Only Yang et al. [29] and Hu et al. [30] have studied the thermodynamic performance of binary R717-based mixtures in Rankine cycle-based OTEC systems. As mentioned earlier, R717's toxicity, flammability, and corrosiveness present challenges and may add unnecessary costs to OTEC applications. Therefore, the use of zeotropic organic refrigerant mixtures in OTEC systems hold great promise and could lead to significant advancements in the field.

In summary, the simple and reliable Rankine cycle remains the preferred choice for OTEC engineering applications, and zeotropic mixtures have the potential to enhance the thermodynamic performance of Rankine cycle-based OTEC systems. However, existing research has primarily focused on R717-based mixtures. Given the potential hazards posed by R717's toxicity, flammability, and corrosiveness in OTEC applications, this study proposes the use of non-toxic and environmentally friendly organic mixtures. Specifically, two R32-based organic mixtures, R32/R125 and R32/R143a, are selected. The thermodynamic and economic models of the

OTEC system are developed to analyze the system's thermodynamic performance (including thermal efficiency and power output) and economic feasibility (including total costs and leveled cost of electricity) under different mass fractions and evaporation temperatures.

2. System description

2.1. OTEC system

As shown in Fig. 1, the illustration of the OTEC system primarily features a series of components including a pump for the working fluid, an evaporator, a turbine, and a condenser. Additionally, it incorporates pumps for both warm and cold seawater, along with pipelines for transporting the fluid. The basic operating principle is as follows: the condensed organic fluid, at low pressure and in a saturated liquid state, is transported from the condenser to the evaporator. In the evaporator, it undergoes heating by absorbing thermal energy from the warm seawater surface, and a phase change into high-temperature and high-pressure steam. This steam then enters the turbine, where it expands and generates electricity. Following the expansion, the exhaust steam is channeled towards the condenser. Here, it undergoes a transformation back into a low-pressure saturated liquid, facilitated by the intense chill of deep-sea water., completing the cycle.

2.2. Selection principle of working fluid

Fig. 2 gives the T-s diagrams for the pure working fluid OTEC and the zeotropic working fluid OTEC. Note: The T-s diagrams here do not contain specific data and are used only for qualitative illustration. Due to the non-isothermal phase change (temperature glide) characteristic, the OTEC using zeotropic mixtures as the working fluid has a better temperature match in the evaporator and condenser compared to the OTEC using pure substances as the working fluid (see Fig. 2), which contributes to the reduction of irreversible losses in the heat exchangers. Therefore, it has become a consensus that zeotropic mixtures applied to OTEC have thermodynamic advantages, which motivates this work.

In general, R717 is widely recognized as a suitable working fluid for OTEC, but it is toxic, flammable and corrosive. Therefore, this paper considers the search for an organic refrigerant as the first component of a zeotropic working fluid. For environmental and ecological considerations, this organic refrigerant must have an ODP of 0, a GWP that is sufficiently small, and be non-toxic and non-corrosive. As a typical representative of third-generation refrigerants, R32 perfectly meets the requirements and is therefore chosen as the first component of the organic non-azeotropic working fluid. In addition, for the simple structure of the OTEC system (without additional distillation equipment), the zeotropic working fluid, which is a combination of the first and second components, must be completely evaporated in the evaporator, which requires that its glide temperature must not be too large. After comprehensive consideration, the third-generation refrigerants R125 and R134a are selected as alternative second components. The thermophysical properties of the three organic refrigerants were listed in Table 1, and the variation of the glide temperatures of two zeotropic working fluids R32/R134a and R32/R125 with the mass fraction of R32 is shown in Fig. 3. From the figure, it can be seen that compared with R32/R125, R32/R134a has a larger glide temperature, but its maximum value is not more than 6 °C, which meets the requirement that the glide temperature should not be too large. It is also worth noting that the maximum glide temperature of R32/R125 does not exceed 1 °C, which is very close to the azeotropic work material, which creates a natural comparison with R32/R134a. Different glide temperatures improve the thermal matching of the heat transfer process to varying degrees. Therefore, it's essential to elucidate how mixed working fluids affect the efficiency of the cycle in terms of thermodynamics.

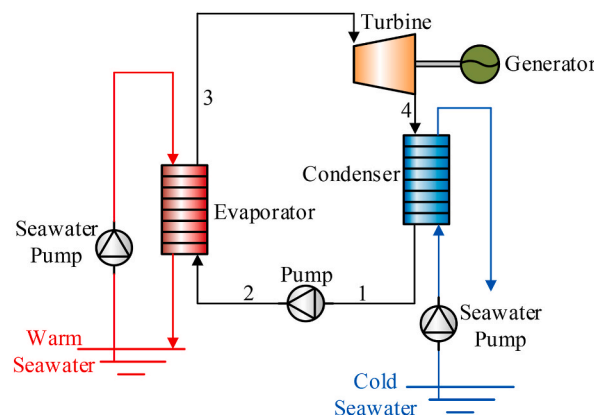


Fig. 1. Schematic diagram of the OTEC system.

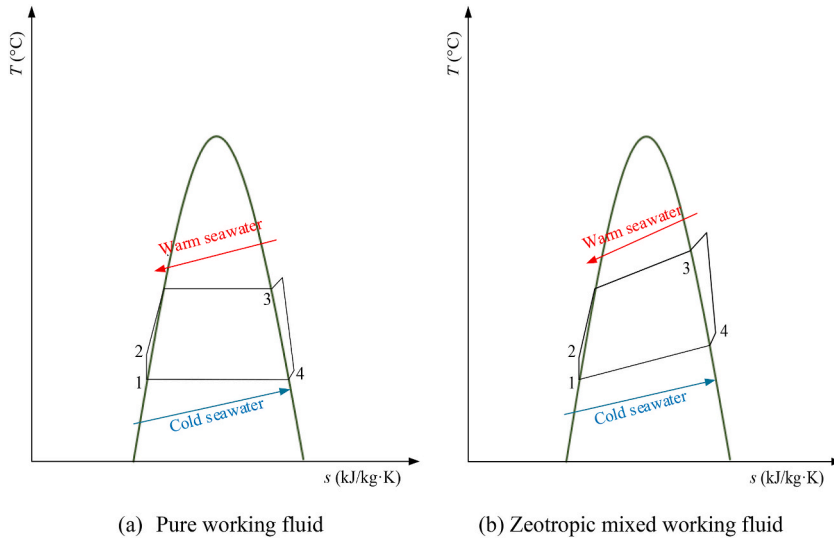


Fig. 2. T-s diagram of the OTEC system.

Table 1
Thermal physical properties of the alternative component [31].

Cycle fluid	Relative molecular mass	Critical temperature $T_c/^\circ\text{C}$	Critical pressure p_c/MPa	ODP	GWP	Security
R32	52.02	78.11	5.78	0	677	A2L
R125	120.02	66.02	3.62	0	3170	A1
R134a	102.03	101.06	4.06	0	1430	A1

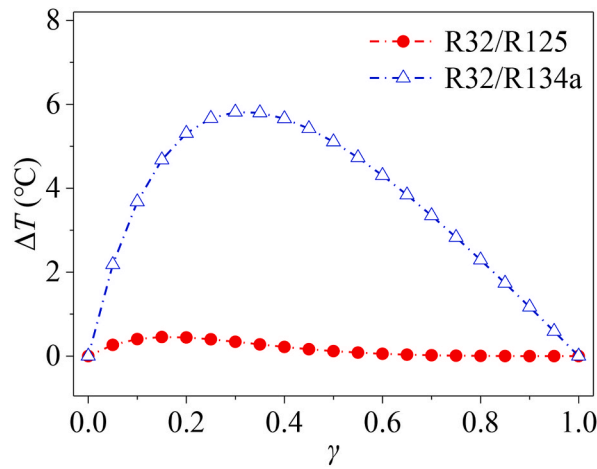


Fig. 3. Temperature glide curve (dew-point temperature of 28 °C).

3. Mathematical models

To assess the viability of the OTEC system with zeotropic working fluids, developing its thermodynamic and economic models is essential. For ease of calculation, some basic assumptions are made as follows [32]:

- (1) The system functions under a stable condition.
- (2) This study disregards the working fluid’s kinetic and potential energies, along with the friction losses in the pipeline.
- (3) Heat losses in the pipelines and equipment within the system are ignored.
- (4) The mixed working fluid maintains a steady composition throughout the entire cycle.
- (5) It is assumed that there is no loss of working fluid from the components.

3.1. Thermodynamic model

The system's thermodynamic model is constructed utilizing the first law of thermodynamics, focusing specifically on the evaporator:

$$Q_E = m_{wf}(h_3 - h_2) = m_{ws}c_{ws}(T_{ws,in} - T_{ws,out}) \quad (1)$$

For the condenser,

$$Q_C = m_{wf}(h_4 - h_1) = m_{cs}c_{cs}(T_{cs,out} - T_{cs,in}) \quad (2)$$

Moreover, we explore the turbine's performance, focusing on its output work and isentropic efficiency. These parameters are crucial for understanding the turbine's energy conversion efficiency and its overall contribution to the system's thermodynamic cycle.

$$W_t = m_{wf}(h_3 - h_4) \quad (3)$$

$$\eta_t = (h_3 - h_4) / (h_3 - h_{4s}) \quad (4)$$

where, η_t denotes the isentropic efficiency of turbine.

The energy usage and the efficiency of the working fluid pump, when operating under ideal conditions, can be characterized in the following manner:

$$W_p = m_{wf}(h_2 - h_1) \quad (5)$$

$$\eta_p = (h_{2s} - h_1) / (h_2 - h_1) \quad (6)$$

where, h_{2s} denotes the theoretical specific enthalpy of isentropic nature expected at the pump's discharge point, and η_p is the isentropic efficiency of pump.

Unlike other ORC power generation systems, the OTEC system needs to draw cold seawater from a depth of 800–1000 meters below sea level. Consequently, the decline in pressure within the marine pipeline, alongside the energy utilization of the seawater pump, warrants significant attention. The latter aspect can be delineated as follows:

$$W_{p,ws/cs} = \frac{m_{ws/cs} \Delta p_{ws/cs}}{\rho_{ws/cs} \eta_{p,ws/cs}} \quad (7)$$

where, $\Delta p_{ws/cs}$ denotes combined pressure loss for combined warm/cold seawater pathway.

The overall decline in pressure experienced by warm seawater during its transport is the sum of the pressure reduction within the seawater pipeline and the drop occurring in the evaporator. This can be determined through the following calculation [33]:

$$\Delta p_{ws} = \Delta p_{ws,P} + \Delta p_{ws,E} \quad (8)$$

where, $\Delta p_{ws,P}$ and $\Delta p_{ws,E}$ represent warm seawater piping pressure drop and evaporator pressure drop, respectively.

The total pressure drop in the warm seawater pipeline can be calculated as follows:

$$\Delta p_{ws,P} = \Delta p_{ws,SP} + \Delta p_{ws,B} \quad (9)$$

where $\Delta p_{ws,B}$ is the loss in the curved section, and $\Delta p_{ws,SP}$ denotes the loss due to friction within the section of the pipe that is straight.

$$\Delta p_{ws,SP} = f \frac{\rho_{ws} L_{ws} v_{ws}^2}{2D_{WP}} \quad (10)$$

where, f is the Fanning friction factor, obtained from the Colebrook-White equation [34]:

$$\frac{1}{\sqrt{f}} = -2 \log \left(\frac{2.51}{Re \sqrt{f}} + \frac{K/D_{WP}}{3.72} \right) \quad (11)$$

where, D_{WP} is the diameter of the seawater pipe.

The curved segment of the warm seawater pipeline experiences a reduction in pressure ($\Delta p_{ws,B}$) can be calculated as follows

$$\Delta p_{ws,B} = f_B \rho_{ws} v_{ws}^2 / 2 \quad (12)$$

where, f_B is the total loss coefficient.

The pressure decrease experienced by the warm seawater within the evaporator ($\Delta p_{ws,E}$) is determined using the following method [35].

$$\Delta p_{ws,E} = \Delta p_{ws,FE} + \Delta p_{ws,ME} + \Delta p_{ws,GE} \quad (13)$$

where, $\Delta p_{ws,FE}$, $\Delta p_{ws,ME}$, and $\Delta p_{ws,GE}$ denote the friction pressure drop, inlet and outlet pressure drop and gravity pressure drop, respectively.

The pressure drop across the evaporator's inlet and outlet is represented as follows:

$$\Delta p_{ws,ME} = 1.5\rho_{ws}v_{ws}^2/2 \quad (14)$$

The friction pressure drop inside the evaporator can be expressed as follows:

$$\Delta p_{ws,FE} = 4f_E \frac{\rho_{ws}L_E v_E^2}{2D_E} \quad (15)$$

where, L_E is the pipeline length, D_E is the hydraulic diameter, and f_E is the friction factor inside the evaporator, calculated by the following equation [35]:

$$f_E = 2.48Re^{-0.20} \quad (16)$$

The pressure drop in the cold seawater pipeline is determined by the following criteria:

$$\Delta p_{cs} = \Delta p_{cs,p} + \Delta p_{cs,c} + \Delta p_{cs,d} \quad (17)$$

where, $\Delta p_{cs,p}$ is the pressure drop in the cold seawater pipeline, $\Delta p_{cs,c}$ is the condenser's pressure drop, calculated similarly to the evaporator, and the pressure difference, denoted as $\Delta p_{cs,d}$, arises due to the variance in density between warm and cold seawater:

$$\Delta p_{cs,d} = L_{cs}\rho_{cs} \left(1 - \frac{\rho_{ws} + \rho_{cs}}{2\rho_{cs}} \right) g \quad (18)$$

Combining Eqs.(1)–(18), the system's net output power can be succinctly defined as follows:

$$W_{net} = W_t - W_p - W_{p,ws} - W_{p,cs} \quad (19)$$

The system's overall efficiency is described as follows:

$$\eta_{net} = \frac{W_{net}}{Q_E} \quad (20)$$

3.2. Economic model

The main cost of the OTEC system comes from heat exchangers (such as the evaporator and the condenser), turbines, pumps, and seawater pipelines. The modular cost calculation approach [36] is employed to assess the investment expenses of crucial components within the OTEC system, thereby determining the system's overall investment cost.

The cost of the evaporator and condenser can be represented as follows:

$$C_{HX} = \frac{CEPCI}{CEPCI_{2001}} \times F_S \times C_{HX,0} \times [B_{1,HX} + (B_{2,HX} \times F_{M,HX} \times F_{p,HX})] \quad (21)$$

where, $CEPCI$ and $CEPCI_{2001}$ are current chemical engineering plant cost index and 2001 chemical engineering plant cost index, respectively, and $C_{HX,0}$ denote foundational cost of heat exchanger, assuming the use of carbon steel and operation at atmospheric pressure, is determined by its heat transfer area.

$$\log C_{HX,0} = K_{1,HX} + K_{2,HX}(\log A_{HX}) + K_{3,HX}(\log A_{HX})^2 \quad (22)$$

where, A_{HX} represents the heat transfer area, with specific calculation details provided in Appendix A. The pressure correction factor $F_{p,HX}$ can be calculated as follows:

$$\log F_{p,HX} = C_{1,HX} + C_{2,HX}(\log p_{HX}) + C_{3,HX}(\log p_{HX})^2 \quad (23)$$

The pump cost are calculated as follows:

$$C_p = \frac{CEPCI}{CEPCI_{2001}} \times F_S \times C_{p,0} \times [B_{1,p} + (B_{2,p} \times F_{M,p} \times F_{p,p})] \quad (24)$$

where, $C_{p,0}$ is the pump's basic cost, primarily influenced by its power consumption. This simplified approach allows for a more straightforward calculation of pump costs, taking into account the pump's characteristics and operational conditions.

$$\log C_{p,0} = K_{1,p} + K_{2,p}(\log W_p) + K_{3,p}(\log W_p)^2 \quad (25)$$

In addition, the pump's performance is further refined by a pressure correction factor, represented as $F_{p,p}$. This factor is crucial for accurately adjusting the pump's output based on varying pressure conditions.

$$\log F_{P,p} = C_{1,p} + C_{2,p}(\log p_p) + C_{3,p}(\log p_p)^2 \quad (26)$$

The calculation of the turbine's cost is determined by the following method:

$$C_t = \frac{CEPCI}{CEPCI_{2001}} \times F_S \times C_{t,0} \times F_{M,t} \quad (27)$$

where, $C_{t,0}$ denote the fundamental cost of the turbine. This basic cost encompasses the initial expenditures associated with the turbine's production.

$$\log C_{t,0} = K_{1,t} + K_{2,t}(\log W_t) + K_{3,TR}(\log W_t)^2 \quad (28)$$

Considering that the equipment in contact with seawater needs to be resistant to corrosion, titanium material is used for the heat exchangers and seawater pump heads. Additionally, when evaluating the pressure correction factors for each piece of equipment, the equipment's operational pressure is duly considered. The values of the constants involved in the cost calculations are presented in Table 2.

The cost of seawater pipelines is calculated using the six-tenths rule, as follows:

$$\frac{C_{WP}}{C_{ref}} = \frac{CEPCI}{CEPCI_{2011}} \times \left(\frac{L_{WP}}{L_{ref}}\right)^{0.6} \times \left(\frac{D_{WP}}{D_{ref}}\right)^{0.6} \times \left(\frac{m_{WP}}{m_{ref}}\right)^{0.6} \quad (29)$$

In this study, we examine the financial aspects of constructing a seawater pipeline, focusing on its cost implications. The cost of the seawater pipeline (C_{WP}) is influenced by several factors, including the $CEPCI_{2011}$, the pipeline's length (L_{WP}), and its inner diameter (D_{WP}). These elements are crucial in determining the overall expenditure required for the pipeline's development, offering insights into the economic feasibility of such projects, m_{WP} represents the mass flow rate of seawater through the pipeline, and the subscript ref refers to actual engineering data from 2011.

Finally, the total cost associated with the OTEC system is determined by

$$C_{tot} = C_{HX} + C_p + C_t + C_{WP} \quad (30)$$

In contemporary power systems, the levelized cost of electricity (LCOE) [38,39] stands as a pivotal economic analysis tool. It calculates the system's total investment cost against its net power output. Specifically, for the OTEC systems, the LCOE is determined by

$$LCOE = \frac{CRF \times C_{tot} + COM}{W_{net} \times t_{op}} \quad (31)$$

In this study, we examine a system designed to operate for 8000 h annually. Operational and maintenance costs, abbreviated as COM, constitute 1.5 % of the system's overall expenses. Additionally, the Capital Recovery Factor (CRF) is introduced, serving as a key financial metric to assess the system's long-term economic viability.

$$CRF = \frac{ir(1+ir)^{Lt}}{(1+ir)^{Lt} - 1} \quad (32)$$

In this scenario, the annual interest rate, denoted as ir , is established at 5 %, while the term Lt signifies the operational lifespan of the OTEC system, which is determined to be 20 years.

4. Results and discussion

The performance of the OTEC systems employing zeotropic mixtures is notably influenced by certain critical parameters. This paper focuses on exploring how variations in the mixture's concentration ratio and the evaporation temperature (specifically, the dew point temperature) affect both the thermodynamic efficiency and economic viability of these systems. Essential parameter configurations are summarized in Table 3 for reference.

Table 2

The value of the constant coefficient involved in the economic model [37].

Constant	Value	Constant	Value	Constant	Value
F_S	1.70	$C_{2,HX}$	0.00	$C_{1,p}$	-0.3935
$B_{1,HX}$	0.96	$C_{3,HX}$	0.00	$C_{2,p}$	0.3957
$B_{2,HX}$	1.21	$B_{1,p}$	1.89	$C_{3,p}$	-0.00226
$F_{M,HX}$	2.40	$B_{2,p}$	1.35	$F_{M,t}$	3.50
$K_{1,HX}$	4.6656	$F_{M,p}$	2.15	$K_{1,t}$	2.2476
$K_{2,HX}$	-0.1557	$K_{1,p}$	3.3892	$K_{2,t}$	1.4965
$K_{3,HX}$	0.1547	$K_{2,p}$	0.0536	$K_{3,t}$	-0.1618
$C_{1,HX}$	0.00	$K_{3,p}$	0.1538		

Table 3
Basic parameter settings of the system [40,41].

Parameter	Value
Turbine output power(kW)	30
Inlet temperature of the warm seawater (°C)	30
Inlet temperature of the cold seawater (°C)	4
Pinch point temperature difference (°C)	1
Turbine efficiency	0.7–0.85
Efficiency of the working fluid pump	0.8
Efficiency of the seawater pump	0.8
Pipeline length of the warm seawater (m)	200
Pipeline length of the cold seawater(m)	1000

4.1. Mixture concentration ratio

The glide temperature, influenced by the concentration ratio, is crucial in determining both the thermodynamic efficiency and the economic feasibility of OTEC systems utilizing zeotropic mixtures, as illustrated in Fig. 2. The R32 mass fraction represents the concentration ratio for R32/R125 and R32/R134a mixtures. To obtain the optimal concentration ratio, the influence of the R32 mass fraction on system parameters such as pump power consumption, heat exchange and heat transfer area, net output power, net efficiency, and LCOE is studied.

Fig. 4 presents the variation in pump power consumption with R32 mass fraction in an environment where the evaporation temperature is set at 28 °C and the condensation temperature at 8 °C. Fig. 4a illustrates that, the trends of pump power consumption with R32 mass fraction are opposite for the two mixture pairs. For the R32/R125 mixture, pump power consumption decreases as the R32 mass fraction rises, and the performance consistently surpasses the R32/R134a mixture. This difference is primarily due to the physical properties of R32, R125, and R134a. Notably, R125 has the highest pump power consumption at 2.28 kW, followed by R32 at 1.63 kW, and R134a at 0.61 kW. Therefore, increasing the R32 mass fraction is beneficial for reducing the pump power consumption of the R32/R125 mixture, while for the R32/R134a mixture, it has the opposite effect.

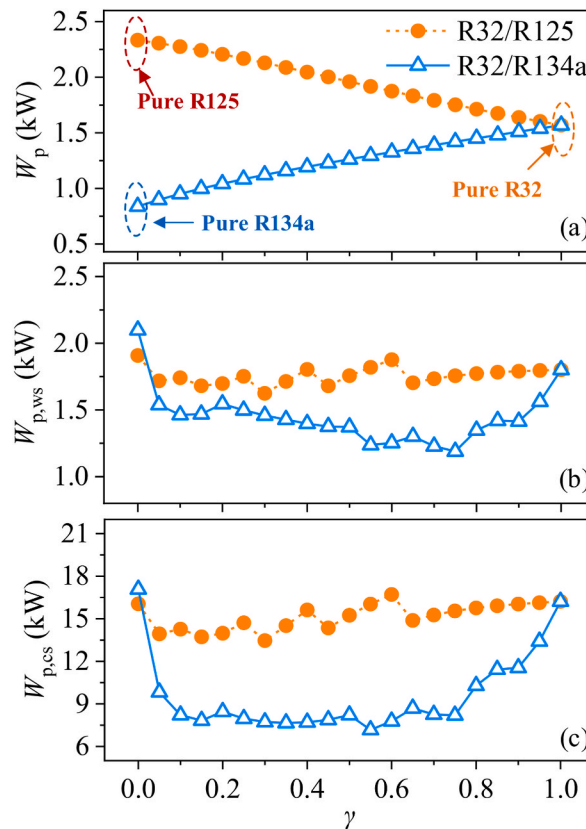


Fig. 4. Effect of the R32 mass fraction on the pump power consumption in the system: (a) working fluid pump, (b) warm seawater pump, and (c) cold seawater pump.

As shown in Fig. 4b and c, the trends in power consumption of the seawater pump with R32 mass fraction are similar for both mixture pairs. In the study of refrigerant mixtures, specifically R32/R125 and R32/R134a, the impact of R32 mass fraction on the seawater pump's power consumption was examined. The findings reveal that the slight variation in glide temperature, under 1 °C, has a negligible influence on the power usage for the R32/R125 blend. Conversely, with the R32/R134a mixture, a noteworthy pattern was observed where the power consumption initially decreases before rising as the R32 mass fraction increases and is always lower than that of the R32/R125 mixture. This is mainly because the improved temperature glide characteristic enhances the temperature match between the liquids surrounding the heat exchanger (including the evaporator and condenser), allowing the seawater to exhibit better heat release/absorption potential (resulting in a larger temperature drop/rise). As a result, the seawater consumption can be reduced and the energy usage of the seawater pump can be effectively reduced. This phenomenon also indicates that in OTEC systems, utilizing zeotropic mixtures due to their temperature glide property significantly lowers the energy required to operate seawater pumps.

The study illustrates how the heat exchange and the area designated for heat transfer in both the evaporator and condenser fluctuate based on the R32 mass fraction, under specific conditions where the evaporation temperature is set at 28 °C and the condensation temperature at 8 °C, as shown in Fig. 5. It was observed that for both equipment, the heat exchange initially rises before it declines, correlating directly with the incremental changes in the R32 mass fraction. The trend becomes more pronounced for the R32/R134a mixture than for the R32/R125 mixture, which is consistent with the change in glide temperature with R32 mass fraction for both mixtures. When the R32 mass fraction is 0.1, the R32/R125 mixture has the highest glide temperature, and the heat exchange also reaches the maximum. Under the specified conditions, the rate at which heat is transferred in both the evaporator and the condenser stands at 702.20 kW and 669.17 kW, respectively. When the R32 mass fraction is 0.3, the R32/R134a mixture has the highest glide temperature, and the heat exchange also reaches the maximum. Under these conditions, the evaporator and condenser achieve heat exchanges of 968.68 kW and 933.21 kW, respectively. The phenomenon observed can be attributed to the effect of glide temperature in systems operating at a constant evaporation temperature, specifically the dew point temperature. The presence of glide temperature plays a role in lowering the overall average temperature throughout the evaporation phase while elevating the average temperature during the condensation phase., thereby reducing the system's thermal efficiency and requiring a larger heat exchange for the same power output. Viewed through this lens, the varying temperature feature of zeotropic mixtures negatively impacts the system.

Fig. 5c and d illustrate that the variations in the regions where heat exchange occurs are largely in agreement, which applies to both the evaporator and the condenser. In the study of refrigerant mixtures, specifically R32/R125 and R32/R134a, the impact on heat transfer efficiency varies significantly with the composition of the mixtures. For the R32/R125 blend, as the proportion of R32 increases, the required heat transfer area diminishes. Conversely, the R32/R134a mixture exhibits a more complex behavior; the heat transfer area initially expands with a rise in R32 content, peaking at 286.33 m² for the evaporator at a 20 % R32 composition. This area further increases for the condenser, reaching its maximum of 342.60 m² at a 25 % R32 composition, before subsequently declining. This pattern indicates a nuanced interaction between the components in the R32/R134a mixture, contrasting the more straightforward relationship seen in the R32/R125 mixture. This phenomenon can also be attributed to the glide temperature.

Fig. 6 shows the variation in key indicators (including net output power, net efficiency, total cost, and LCOE) with R32 mass fraction under the specified parameters with an evaporation temperature at 28 °C and a condensation temperature at 8 °C. The temperature glide characteristic significantly improves the temperature matching of the fluids on both sides of the heat exchanger, which allows seawater to show greater temperature rise/drop in the heat exchanger, thus reducing the power consumption of the seawater pump. As a result, the net power output of R32/R134a with significant temperature glide characteristics is significantly higher than that of pure R32 and R134a. From the data, at a mass fraction of R32 of 0.55, the net power output of the OTEC with R32/

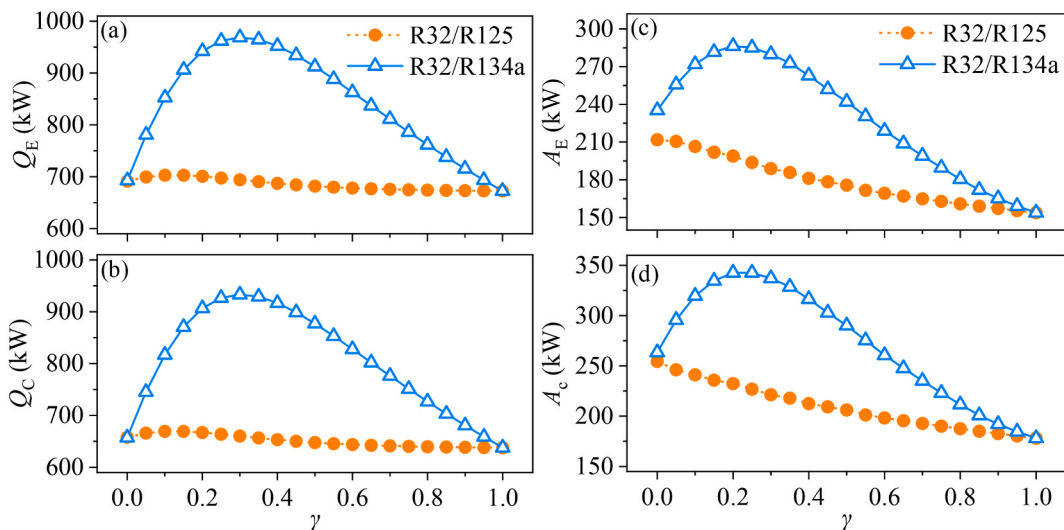


Fig. 5. Effect of R32 mass fraction on heat exchange and heat transfer area: (a) heat exchange of the evaporator, (b) heat exchange of the condenser, (c) heat transfer area of the evaporator, and (d) heat transfer area of the condenser.

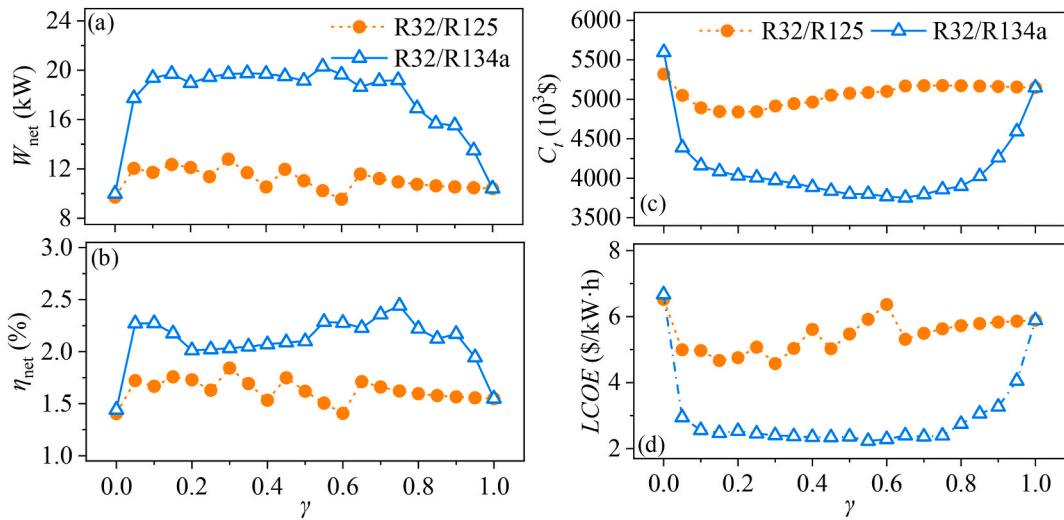


Fig. 6. Effect of R32 mass fraction on heat exchange and heat transfer area: (a) net output power, (b) net efficiency, (c) total cost, (d) LCOE.

R134a is 20.30 kW, which is much larger than that of the pure R32 of 10.43 kW and that of the pure R134a of 10.04 kW. However, due to the small glide temperature of the R32/R125 mixture (less than 1 °C, which is close to the azeotropic mixture), the net output power and net efficiency of the OTEC with R32/R125 are not significantly improved compared to that of pure R32 or pure R125 and are much

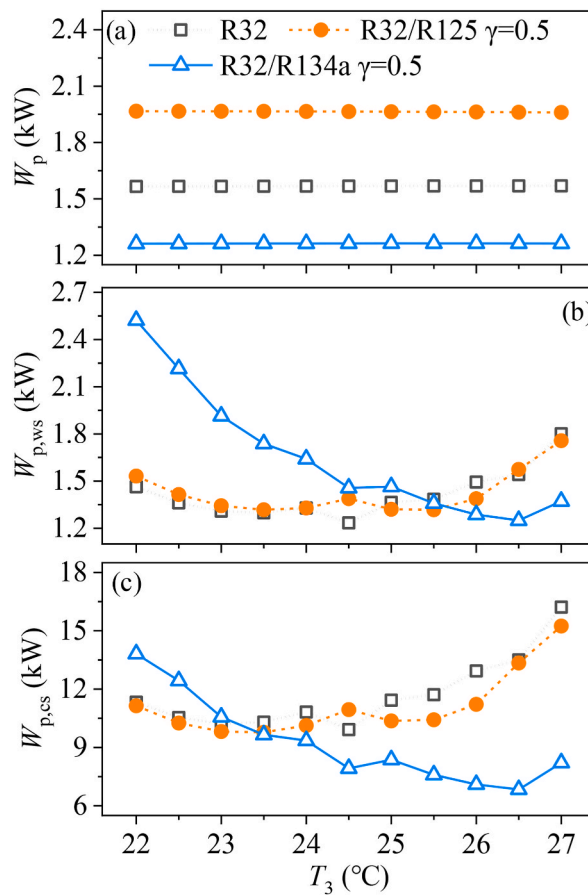


Fig. 7. Effect of evaporation temperature on pump power consumption in the system: (a) working fluid pump, (b) warm seawater pump, and (c) cold seawater pump.

lower than that of the OTEC system with R32/R134a.

In terms of economic performance, even though the OTEC system with R32/R134a, which has significant temperature glide characteristics, has a larger heat transfer area (see Fig. 5), the total cost of the system is still much lower than that of the OTEC with pure working fluid and the OTEC with R32/R125, due to the reduced investment in seawater pumps and seawater piping (since R32/R134a has a higher seawater utilization rate). Furthermore, the LCOE of the OTEC system with R32/R134a is also much lower than that of the OTEC with pure working fluid and that of the OTEC with R32/R125 due to the advantages in both net power output as well as in total cost. At a mass fraction of R32 of 0.4, the LCOE of the OTEC with R32/R134a is 2.36 \$/kWh, while the LCOE of OTEC with R32 as well as R32/R125 is 5.88 \$/kWh and 5.61 \$/kWh, respectively. Therefore, the R32/R134a mixture is the more recommended working fluid, both in terms of thermodynamic and economic performance.

4.2. Evaporation temperature

The evaporation temperature (dew point temperature) is a key design and operating parameter of the system. This study considers three working fluids: R32, R32/R125, and R32/R134a, in a composition where R32 constitutes 50 % of the mass. The focus is on the impact of evaporation temperature (dew point temperature) on system pump power consumption, heat exchange and heat transfer area, net output power, net efficiency, total cost, and LCOE.

Fig. 7 presents the variation of pump power consumption (including pumps of the working fluid and the seawater) with evaporation temperature under a condensation temperature of 8 °C. Fig. 7a illustrates that the energy usage of the pump for three different working fluids remains relatively stable across a temperature range of 22 °C–27 °C, indicating insensitivity to fluctuations in evaporation temperature. For the R32/R134a mixture, it is significantly lower than that for R32 and the R32/R125 mixture. It can be seen from Fig. 7b and c that, the variation trends of power consumption of the seawater pump for systems using R32 and R32/R125 are similar with changes in evaporation temperature because the R32/R125 mixture is close to an azeotropic mixture (glide temperature less than 1 °C). However, the trend for the R32/R134a mixture is different. Additionally, the power consumption of the warm seawater pump for the R32/R134a mixture is higher than that for pure R32 and the R32/R125 mixture when the evaporation temperature is below 25.5 °C. Nevertheless, when the evaporation temperature is below 23.5 °C, the power consumption of the cold seawater pump for the R32/R134a mixture is higher than that for pure R32 and the R32/R125 mixture. It can be observed that the R32/R134a mixture, which has a significant temperature glide, does not always outperform pure R32 and the near-azeotropic R32/R125 mixture in terms of seawater pump power consumption. Therefore, when using the R32/R134a mixture, the evaporation temperature should be as high as possible.

The relationship between the evaporation temperature and the efficiency of heat exchange in both the evaporator and condenser, under a fixed condensation temperature of 8 °C, is illustrated in Fig. 8. It demonstrates that the increment of evaporation temperature results in the enhanced thermal efficiency of the system under steady condensation temperature conditions. This means that for the same turbine output power, the higher the evaporation temperature, the lower the ability of the evaporator and condenser to transfer heat. The data presented in Fig. 8a and b demonstrate a consistent decline in the heat exchange efficiency of the evaporator and condenser across three different working fluids as the evaporation temperature rises from 22 °C to 27 °C. Notably, the R32/R134a mixture outperforms the other two fluids—pure R32 and the R32/R125 mixture—in terms of heat exchange, attributed to its temperature glide properties.

The determination of a heat transfer area is influenced by the heat exchange process and the temperature difference during heat transfer. Raising the evaporation temperature results in lower heat exchange efficiency and a reduced temperature gap, which in turn, impacts the heat transfer area in contradictory ways. Specifically, a reduced heat exchange lowers the required heat transfer area, whereas a diminished temperature difference necessitates a larger area for effective heat transfer. This balance results in varying heat transfer area requirements for evaporators and condensers at different evaporation temperatures, as depicted in Fig. 8c and d. At an evaporation temperature of 25 °C, the heat transfer area reaches its lowest for both the R32/R134a blend (98.38 m²) and pure R32 (88.29 m²). Meanwhile, the R32/R125 mixture attains its minimum required area of 102.38 m² at a slightly higher temperature of 25.5 °C. However, when we consider the condenser, the minimum heat transfer area (93.76 m², 117.82 m², and 108.83 m², respectively) for pure R32, the R32/R125 mixture, and the R32/R134a mixture is reached at an evaporation temperature of 25 °C. Additionally, due to the temperature glide characteristics, the heat transfer area required for the R32/R134a mixture is much larger than that for pure R32 and the R32/R125 mixture.

Fig. 9 exhibits the variation of key performance indicators (including net output power, net efficiency, total cost, and LCOE) with evaporation temperature under a condensation temperature of 8 °C. Fig. 9a illustrates that the system's net output power reaches its peak at an optimal evaporation temperature. The optimal evaporation temperatures for achieving the maximum net output power for pure R32, the R32/R125 mixture, and the R32/R134a mixture are 24.5 °C, 23.5 °C, and 26.5 °C, respectively, with maximum net output powers of 17.28 kW, 16.94 kW, and 20.65 kW, respectively. Similarly, there is an optimal evaporation temperature that maximizes the system's net efficiency, which is 24.5 °C, 26 °C, and 26.5 °C for pure R32, the R32/R125 mixture, and the R32/R134a mixture respectively. The maximum net efficiencies of the system are 1.955 %, 2.046 %, and 2.115 %, respectively. The R32/R134a mixture demonstrates enhanced system performance, showing notable improvements in both net output power and efficiency at elevated evaporation temperatures.

It can be seen that from a total cost perspective, as presented in Fig. 9, increasing the evaporation temperature is unfavorable for systems using pure R32 and the R32/R125 mixture. As the evaporation temperature rises, systems employing the R32/R134a mixture see a gradual reduction in total costs. Notably, at temperatures exceeding 25 °C, these systems become more cost-effective than those using alternative refrigerants. Furthermore, an analysis of Fig. 9d reveals a correlation between the LCOE and total costs across the

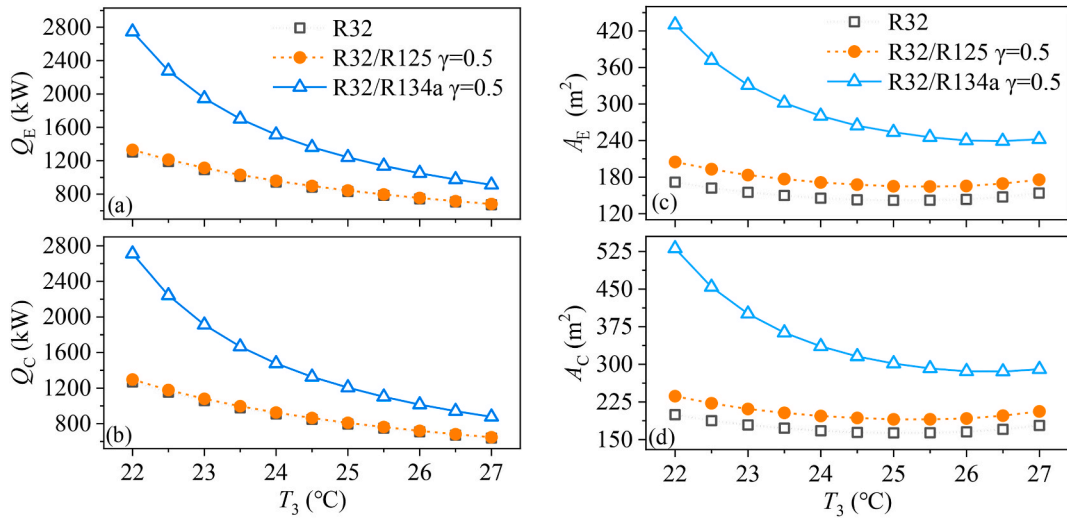


Fig. 8. Effect of evaporation temperature on heat exchange and heat transfer area: (a) heat exchange of the evaporator, (b) heat exchange of the condenser, (c) heat transfer area of the evaporator, and (d) heat transfer area of the condenser.

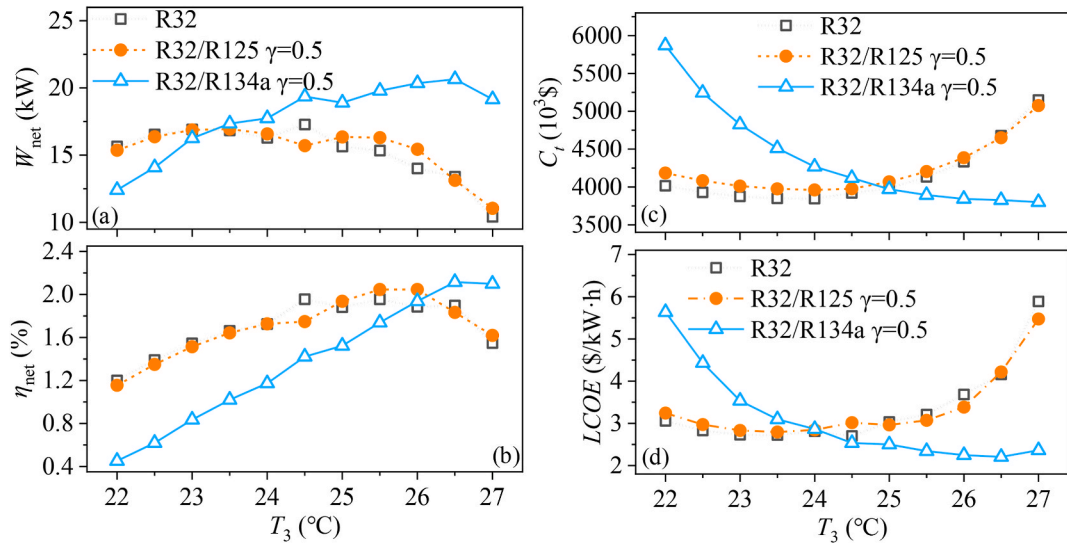


Fig. 9. Effect of evaporation temperature on key performance indicators of the system: (a) net output power, (b) net efficiency, (c) total cost, and (d) LCOE.

three refrigerants, mirroring the trend observed in total cost variations with evaporation temperature. When the evaporation temperature is above 24 °C, the LCOE for the R32/R134a mixture begins to be lower than that for pure R32 and the R32/R125 mixture. Moreover, the LCOE for pure R32 and the R32/R125 mixture is 2.49 times and 2.32 times that for the R32/R134a mixture, respectively at an evaporation temperature of 27 °C.

5. Conclusion

This study examines the efficiency and cost-effectiveness of the OTEC systems utilizing zeotropic mixed working fluids, focusing on R32/R125 and R32/R134a blends. By developing thermodynamic and economic models, it explores how variations in the mixed working fluid's composition and the evaporation temperature influence the system's performance. Key findings include:

- (1) The R32/R134a mixture, with significant temperature glide characteristics, significantly reduces the power usage of the seawater pump, resulting in an increased net power output. At a mass fraction of R32 of 0.55, the net power output of the OTEC

with R32/R134a is 20.30 kW, which is much larger than that of the pure R32 of 10.43 kW and that of the pure R134a of 10.04 kW.

- (2) The use of R32/R134a, which has significant temperature glide characteristics, as the working fluid for OTEC significantly improves the economic performance of the system. At a mass fraction of R32 of 0.4, the LCOE of the OTEC with R32/R134a is 2.36 \$/kWh, while the LCOE of OTEC with R32 as well as R32/R125 is 5.88 \$/kWh and 5.61 \$/kWh, respectively.
- (3) For OTEC systems using R32/R134a, increasing the evaporation temperature is a promising way to improve the thermodynamic and economic performance of the system.

CRedit authorship contribution statement

Yanmei Zhang: Writing – original draft, Software, Investigation, Conceptualization, Data curation, Formal analysis, Methodology. **Jiawei Deng:** Software, Conceptualization, Methodology, Writing – review & editing. **Zilong Deng:** Funding acquisition, Writing – review & editing.

Declaration of competing interest

The authors declare that they have no known competing financial interests or personal relationships that could have appeared to influence the work reported in this paper.

Acknowledgments

The authors would like to appreciate the funding support of the National Natural Science Foundation of China (Nos. 92373118 & 52276054) and Zhishan Scholar Program of Southeast University (2242023R40004, China).

Appendix A. Calculation of the heat exchanger area

Within the framework of OTEC systems, the temperature variance for heat transfer is notably slight, compact heat exchangers emerge as the optimal solution. Specifically, the plate heat exchanger has been identified as the most suitable for both the evaporator and condenser roles when working with zeotropic mixed fluids. This selection is informed by the need for efficiency, assuming uniformity in plate parameters such as a 0.6 mm thickness and a 60°V-shaped angle. The sizing of the heat exchanger, guided by established models (see Ref. [42]), takes into account the phase change of the working fluid. This necessitates a division into single-phase and two-phase sections for precise calculation, each governed by a consistent energy balance equation.

$$Q = U \cdot A \cdot LMTD \quad (A1)$$

In exploring how heat is exchanged, we focus on three essential elements: the area available for heat transfer (A), the average temperature difference calculated logarithmically (LMTD) between the working fluid and seawater throughout the heat exchange areas, and the comprehensive heat transfer rate (U). The latter is a calculated value that encapsulates the heat transfer efficiency across the designated area. This document is designed to offer a succinct summary of the interaction between various elements that enable heat transfer, emphasizing their roles and interrelations within the context of thermal engineering.

$$\frac{1}{U} = \frac{1}{\alpha_{wf}} + \frac{\delta}{\lambda} + \frac{1}{\alpha_{sw}} \quad (A2)$$

In the study of heat exchangers, the efficiency of heat transfer is crucial. This is characterized by the plate's thickness (δ) and its thermal conductivity (λ), along with the convective heat transfer coefficients for both the working fluid (α_{wf}) and seawater (α_{sw}). These coefficients are determined through specific heat transfer correlations, highlighting the interaction between the materials and the fluids involved.

For the single-phase section (including the working fluid and seawater, the heat transfer correlation is [43].

$$\alpha = 0.724 \left(\frac{6\beta}{\pi} \right)^{0.646} Re^{0.583} Pr^{1/3} \frac{\lambda}{D_E} \quad (A3)$$

where, β is the plate corrugation angle, Re is the Reynolds number, and Pr is the Prandtl number.

For the two-phase section inside the evaporator, the heat transfer correlation is as follows [44]:

$$\alpha_{eva} = 5.323 Re_{eq}^{0.42} Pr_l^{1/3} \frac{\lambda_l}{D_E} \quad (A4)$$

We examine the thermal performance of saturated liquid working fluids, focusing on two key parameters: the Prandtl number (Pr_l) and thermal conductivity (λ_l). Additionally, we introduce the concept of the equivalent Reynolds number (Re_{eq}), a crucial factor in understanding fluid dynamics within this context. The Re_{eq} is determined using a specific calculation method outlined in our methodology section. This approach allows for a more nuanced analysis of heat transfer processes, providing insights into the optimization

of thermal systems.

$$Re_{eq} = \frac{G_{eq} D_E}{\mu_l} \quad (A5)$$

where, μ_l is the dynamic viscosity of the saturated liquid working fluid, and G_{eq} is the equivalent mass flux, which can be calculated as follows:

$$G_{eq} = G \left(1 - x + x \left(\frac{\rho_l}{\rho_g} \right)^{0.5} \right) \quad (A6)$$

In the context of thermal systems, understanding the relationship at the interface of liquid and vapor states is crucial. This relationship is quantified by the densities of the saturated liquid (ρ_l) and gas (ρ_g) states of the fluid, alongside the dryness fraction (x), which indicates the proportion of gas in the mixture. Additionally, the mass flux (G) plays a pivotal role, representing the rate at which mass flows through a given area. This interplay between the liquid and gas densities, the dryness fraction, and the mass flux is fundamental in analyzing and optimizing the performance of thermal systems.

In the condenser's two-phase region, the following formula represents the heat transfer correlation [45]:

$$\alpha_{cond} = 4.118 Re_{eq}^{0.4} Pr_l^{1/3} \frac{\lambda_l}{D_E} \quad (A7)$$

Data availability

Data will be made available on request.

References

- [1] Y. Du, H. Peng, J. Xu, Z. Tian, Y. Zhang, X. Han, et al., Performance analysis of ocean thermal energy conversion system integrated with waste heat recovery from offshore oil and gas platform, *Case Stud. Therm. Eng.* 54 (2024) 104027.
- [2] S. Li, Y. Zhang, Z. Zhou, W. Shi, J. Zhang, B. Wang, Study on improving the storage efficiency of ocean thermal energy storage (OTES) unit by using fins, *Case Stud. Therm. Eng.* 37 (2022) 102262.
- [3] J. Herrera, S. Sierra, A. Ibeas, Ocean thermal energy conversion and other uses of deep sea water: a review, *J. Mar. Sci. Eng.* 9 (4) (2021).
- [4] A. Gupta, V.S. Sankhla, D. Sharma, A comprehensive review on the sustainable refrigeration systems, *Mater. Today: Proc.* 44 (2021) 4850–4854.
- [5] F. Chen, L. Liu, J. Peng, Y. Ge, H. Wu, W. Liu, Theoretical and experimental research on the thermal performance of ocean thermal energy conversion system using the rankine cycle mode, *Energy* 183 (2019) 497–503.
- [6] W. Liu, X. Xu, F. Chen, Y. Liu, S. Li, L. Liu, et al., A review of research on the closed thermodynamic cycles of ocean thermal energy conversion, *Renew. Sustain. Energy Rev.* 119 (2020).
- [7] M. Wang, R. Jing, H. Zhang, C. Meng, N. Li, Y. Zhao, An innovative Organic Rankine Cycle (ORC) based Ocean Thermal Energy Conversion (OTEC) system with performance simulation and multi-objective optimization, *Appl. Therm. Eng.* 145 (2018) 743–754.
- [8] W. Xu, R. Zhao, S. Deng, L. Zhao, S.S.J.R. Mao, S.E. Reviews, Is Zeotropic Working Fluid a Promising Option for Organic Rankine Cycle: A Quantitative Evaluation Based on Literature Data, vol. 148, 2021 111267.
- [9] G.B. Abadi, K.C.J.R. Kim, S.E. Reviews, Investigation of Organic Rankine Cycles with Zeotropic Mixtures as a Working Fluid: Advantages and Issues, vol. 73, 2017, pp. 1000–1013.
- [10] S.M. Abbas, H.D.S. Alhassany, D. Vera, F. Jurado, Review of enhancement for ocean thermal energy conversion system, *J. Ocean Eng. Sci.* 8 (5) (2023) 533–545.
- [11] A.I. Kalina, Combined-cycle system with novel bottoming cycle, *J. Eng. Gas Turbines Power* 106 (4) (1984) 737–742.
- [12] Uehara HjtOJ, B. Series, Performance analysis of OTEC system using a cycle with absorption and extraction processes 64 (624) (1998) 384–389.
- [13] J. Zhang, X. Zhang, Z. Zhang, P. Zhou, Y. Zhang, H. Yuan, Performance improvement of ocean thermal energy conversion organic Rankine cycle under temperature glide effect, *Energy* 246 (2022) 123440.
- [14] M. Wang, R. Jing, H. Zhang, C. Meng, N. Li, Y. Zhao, An innovative Organic Rankine Cycle (ORC) based Ocean Thermal Energy Conversion (OTEC) system with performance simulation and multi-objective optimization, *Appl. Therm. Eng.* 145 (2018) 743–754.
- [15] N.-J. Kim, S.-H. Shin, W.-G. Chun, A study on the thermodynamic cycle of OTEC system 26 (2) (2006) 9–18.
- [16] D. Rosard, Generalized Parameters for Selection of Turbines and Working Fluids for OTEC Power Systems, 1980.
- [17] F. Sun, Y. Ikegami, B. Jia, H. Arima, Optimization design and exergy analysis of organic rankine cycle in ocean thermal energy conversion, *Appl. Ocean Res.* 35 (2012) 38–46.
- [18] J.-I. Yoon, C.-H. Son, S.-M. Baek, H.-J. Kim, H.-S. Lee, Efficiency comparison of subcritical OTEC power cycle using various working fluids, *Heat Mass Tran.* 50 (7) (2014) 985–996.
- [19] H. Wang, H.J.O.E. Wang, Selection of working fluids for ocean thermal energy conversion power generation organic Rankine cycle 27 (2) (2009) 119–123.
- [20] W. Chunxu, W. Bijun, Y.J.R.E.R. Yin, Analysis of zeotropic mixtures used in OTEC Rankine cycle system 33 (4) (2015) 621–636.
- [21] J. Gong, T. Gao, Li Gijosee, Performance analysis of 15 kW closed cycle ocean thermal energy conversion system with different working fluids 135 (2) (2013) 024501.
- [22] Ikegami Y, Goto H, Morisaki T, Furukawa T. Effect of working fluid flow rate and ammonia concentration on OTEC using ammonia/water mixture as working fluid. *Conference Effect of Working Fluid Flow Rate and Ammonia Concentration on OTEC Using Ammonia/water Mixture as Working Fluid.* p. 1026-1029.
- [23] F. Alshammari, I. Alatawi, A.S. Alshammari, Impact of turbine characteristics on low temperature organic Rankine cycles operating with zeotropic and azeotropic mixtures, *Case Stud. Therm. Eng.* 59 (2024) 104463.
- [24] M. Zhan, I.B. Mansir, P.K. Singh, H. Rajab, A.M. Abed, M. Dahari, et al., Thermal process simulation and multi-variable study/optimization of a novel geothermal-driven multi-generation process using bi-evaporator with zeotropic mixture, *Case Stud. Therm. Eng.* 43 (2023) 102790.
- [25] M. Kolahi, M. Yari, S.M.S. Mahmoudi, F. Mohammadkhani, Thermodynamic and economic performance improvement of ORCs through using zeotropic mixtures: case of waste heat recovery in an offshore platform, *Case Stud. Therm. Eng.* 8 (2016) 51–70.

- [26] M.H. Yang, R.H. Yeh, Optimum composition ratios of multicomponent mixtures of organic Rankine cycle for engine waste heat recovery 44 (2) (2020) 1012–1030.
- [27] Q. Liu, A. Shen, Y. Duan, Parametric optimization and performance analyses of geothermal organic Rankine cycles using R600a/R601a mixtures as working fluids, *Appl. Energy* 148 (2015) 410–420.
- [28] A.H. Mosaffa, L.G. Farshi, Thermodynamic feasibility evaluation of an innovative salinity gradient solar ponds-based ORC using a zeotropic mixture as working fluid and LNG cold energy, *Appl. Therm. Eng.* 186 (2021) 116488.
- [29] M.-H. Yang, R.-H. Yeh, Investigation of the potential of R717 blends as working fluids in the organic Rankine cycle (ORC) for ocean thermal energy conversion (OTEC), *Energy* 245 (2022) 123317.
- [30] Z. Hu, Y. Chen, C. Zhang, Role of R717 blends in ocean thermal energy conversion organic Rankine cycle, *Renew. Energy* 221 (2024) 119756.
- [31] C. Bernardoni, M. Binotti, A. Giostri, Techno-economic analysis of closed OTEC cycles for power generation, *Renew. Energy* 132 (2019) 1018–1033.
- [32] C. Li, L. Pan, Y. Wang, Thermodynamic optimization of Rankine cycle using CO₂-based binary zeotropic mixture for ocean thermal energy conversion, *Appl. Therm. Eng.* 178 (2020).
- [33] H. Uehara, Y. Ikegami, Optimization of a Closed-Cycle OTEC System, 1990.
- [34] E.S. Menon, *Transmission Pipeline Calculations and Simulations Manual*, Gulf Professional Publishing, 2014.
- [35] K. Nilpueng, T. Keawkamrop, H.S. Ahn, S. Wongwises, Effect of chevron angle and surface roughness on thermal performance of single-phase water flow inside a plate heat exchanger, *Int. Commun. Heat Mass Tran.* 91 (2018) 201–209.
- [36] R. Turton, R.C. Bailie, W.B. Whiting, J.A. Shaeiwitz, *Analysis, Synthesis and Design of Chemical Processes*, Pearson Education, 2008.
- [37] L. Pan, Y. Ma, T. Li, H. Li, B. Li, X. Wei, Investigation on the cycle performance and the combustion characteristic of two CO₂-based binary mixtures for the transcritical power cycle, *Energy* 179 (2019) 454–463.
- [38] R. Salcedo, E. Antipova, D. Boer, L. Jiménez, G. Guillén-Gosálbez, Multi-objective optimization of solar Rankine cycles coupled with reverse osmosis desalination considering economic and life cycle environmental concerns, *Desalination* 286 (2012) 358–371.
- [39] E. Cayer, N. Galanis, H. Nesreddine, Parametric study and optimization of a transcritical power cycle using a low temperature source, *Appl. Energy* 87 (4) (2010) 1349–1357.
- [40] M. Li, J. Wang, S. Li, X. Wang, W. He, Y. Dai, Thermo-economic analysis and comparison of a CO₂ transcritical power cycle and an organic Rankine cycle, *Geothermics* 50 (2014) 101–111.
- [41] J.-I. Yoon, S.-H. Seol, C.-H. Son, S.-H. Jung, Y.-B. Kim, H.-S. Lee, et al., Analysis of the high-efficiency EP-OTEC cycle using R152a, *Renew. Energy* 105 (2017) 366–373.
- [42] S. Quoilin, S. Declaye, B.F. Tchanche, V. Lemort, Thermo-economic optimization of waste heat recovery Organic Rankine Cycles, *Appl. Therm. Eng.* 31 (14) (2011) 2885–2893.
- [43] K. Nilpueng, S. Wongwises, Experimental study of single-phase heat transfer and pressure drop inside a plate heat exchanger with a rough surface, *Exp. Therm. Fluid Sci.* 68 (2015) 268–275.
- [44] I.-K. Kim, J.-H. Park, Y.-H. Kwon, Y.-S. Kim, Experimental study on R-410A evaporation heat transfer characteristics in oblong shell and plate heat exchanger 28 (7) (2007) 633–639.
- [45] Y.-Y. Yan, H.-C. Lio, T.-F. Lin, Condensation heat transfer and pressure drop of refrigerant R-134a in a plate heat exchanger, *Int. J. Heat Mass Tran.* 42 (6) (1999) 993–1006.